

## Tuning the Architecture of Mesostructures by Electrodeposition

Zhi-Li Xiao,\* Catherine Y. Han, Wai-Kwong Kwok, Hsien-Hau Wang, Ulrich Welp, Jian Wang, and George W. Crabtree

Materials Science Division, Argonne National Laboratory, Argonne, Illinois 60439

Received December 4, 2003; E-mail: xiao@anl.gov

The physical and chemical properties of mesostructures<sup>1</sup> depend on their architectures, including geometry, morphology and hierarchical structures, and can be fine-tuned by controlling these parameters.<sup>2,3</sup> The synthesis of mesostructures with well-controlled architectures opens new pathways for the development of future nanodevices. Various methods including template synthesis,<sup>4,5</sup> vapor deposition,<sup>6</sup> and colloidal synthesis<sup>7,8</sup> have demonstrated success in fabricating certain architectures, such as cylindrical cobalt nanowires,<sup>5</sup> triangular platinum<sup>2</sup> and cubic silver<sup>8</sup> nanoparticles, zinc oxide in the forms of nanobelts, nanosprings, and other novel hierarchical nanostructures.<sup>9,10</sup> Here we show that electrodeposition<sup>1,11</sup> can provide versatility in tailoring the architectures of mesostructures. Novel lead (Pb) mesostructures ranging from nanowires with cylindrical and square cross sections to mesoparticles with triangular, hexagonal, octahedral, decahedral, and icosahedral shapes and complicated structures such as multipods, porous nanowires, nanobrushes, and snowflakes were synthesized through systematically exploring electrodeposition parameters.

To obtain individual particles or clusters, the surface energy of the substrate (working electrode) needs to be much smaller than that of the deposits, leading to island formation through a Volmer–Weber growth mode.<sup>1</sup> All the results reported here were obtained by using the basal planes of highly oriented pyrolytic graphite (HOPG) as substrates. The architecture of the deposits is strongly affected by the growth rate, controlled by the electrolyte concentration. The best concentration range for growing lead mesostructures with controlled architectures is from 1 to 10 mM (most experiments were carried out with a concentration of 5 mM). Hydrogen evolution resulting from the proton reduction is very sensitive to the pH value of the solution, which can be adjusted by the supporting electrolyte. Macroscopic hydrogen bubbles could be seen at reduction potential below  $-1$  V when the pH value was below 3. The supporting electrolyte we used is boric acid with a pH value of 4.80 at a concentration of 0.1 M.

Scanning electron microscopy images of mesostructures obtained at various reduction potentials with starting materials of lead nitrate and lead acetate are delineated in Figures 1 and 2, respectively. In general, mesoparticles (icosahedron, decahedron, and octahedron in Figure 1a–c; icosahedron, decahedron, hexagon, and triangle in Figure 2a–d, respectively) form at applied voltages close to the thermodynamic equilibrium potential, while nanowires (Figures 1d,e and 2g), nanobrushes (Figures 1f and 2h), and monopods and multipods (Figure 2e,f) are obtained at high reduction potentials. However, there are differences in the morphology of the deposits, depending on the starting material. For example, the surfaces of the mesoparticles initiated with lead nitrate are considerably smoother than those obtained with lead acetate. The cross sections of the nanowires are square with lead acetate and cylindrical with lead nitrate precursors. The symmetry of the nanobrushes changes from random to four-fold when lead nitrate is replaced with lead acetate or lead chloride (left panel in the graphic shown on the

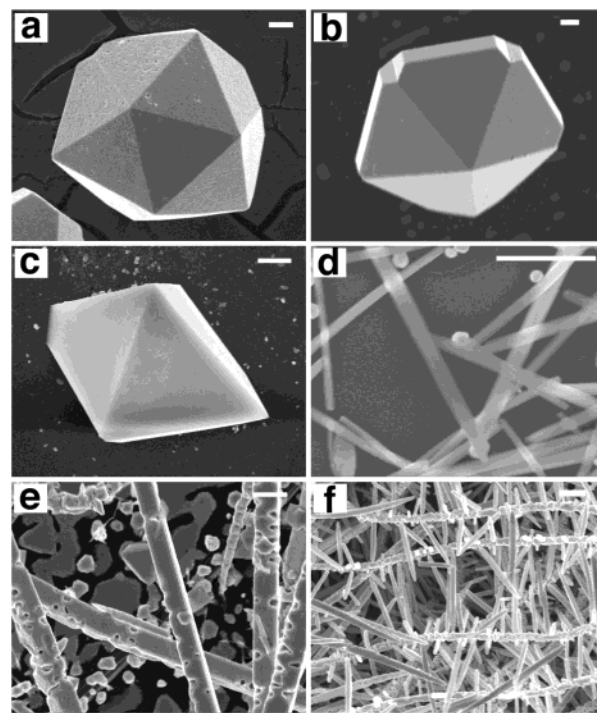


**Figure 1.** Architecture evolution with applied potential for solution containing 5 mM lead nitrate and 0.1 M boric acid. The reduction potentials for a–f are  $-0.8$ ,  $-0.95$ ,  $-1.1$ ,  $-1.2$ ,  $-1.7$ , and  $-2.0$  V, respectively. The scale bar length is 500 nm. The growth time is 60 s.

Table of Contents for this Communication). Furthermore, mesostructures such as monopods and multipods appear only in solution containing acetate or chloride.

The shape evolution from mesoparticles to nanowires and multipods with increasing reduction potentials parallels the findings in colloidal synthesis,<sup>7</sup> where the formation of nanowires and other elongated structures requires an environment with a high electrochemical potential achieved with high monomer concentrations. In electrodeposition, the reduction potential equals the electrochemical potential of the electrode and that of the deposited materials. With increasing reduction potential, structures with higher chemical potential and higher aspect ratio such as nanowires are expected to form on the cathode. In fact, the appearance of mesoparticles follows the sequence of their specific surface energies that determine their chemical potentials. For example, icosahedra-shaped mesoparticles appear at the lowest reduction potential because an icosahedron has the lowest specific surface energy, followed by a decahedron.<sup>12</sup> In colloidal synthesis, some capping molecules can block certain faces and enhance growth of other facets, leading to the formation of multipods at high monomer concentration. The electrodeposited multipods shown in Figure 2 indicate that acetic and chloric anions have similar preference for certain facets of the lead structure and serve as effective capping agents.

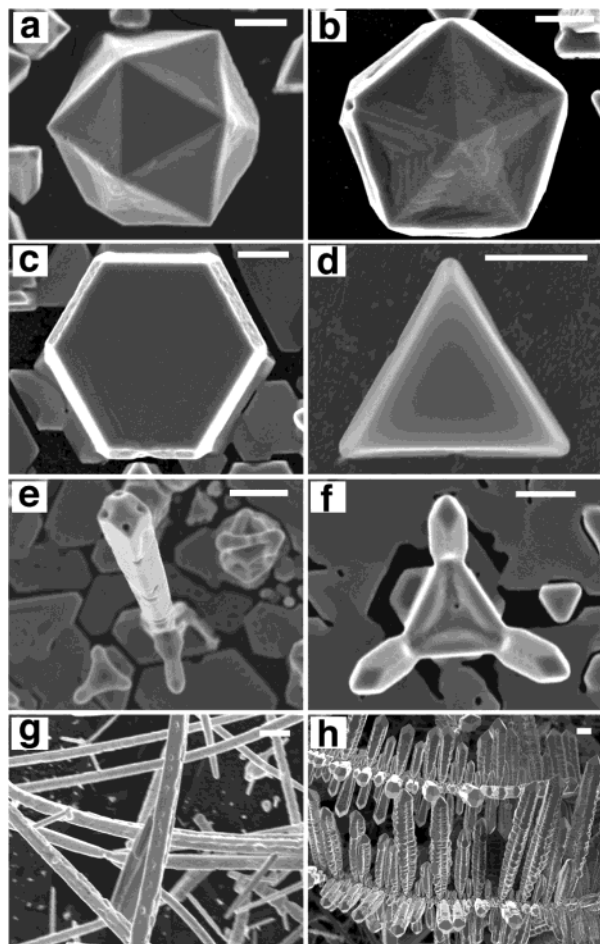


**Figure 2.** Architecture evolution with reduction potential for solution containing 5 mM lead acetate and 0.1 M boric acid. The reduction potentials for a–h are  $-0.65$ ,  $-0.8$ ,  $-1.0$ ,  $-1.1$ ,  $-1.3$ ,  $-1.4$ ,  $-1.6$ , and  $-1.9$  V, respectively. The scale bar length is 500 nm. The growth time is 60 s.

The novel shapes of icosahedron, decahedron, and octahedron lead mesostructures obtained at applied voltages close to the equilibrium potential can be understood with a model based on a modified Wulff construction for shape formation used to interpret the organization of thermally annealed gold and silver particles and clusters of inert gas atoms.<sup>12</sup> According to this model, which minimizes the total surface and twin-boundary energies of an assembly of single-crystal units at constant volume, the polyhedra can be described as a collection of single-crystal tetrahedra that are twin-related at their adjoining faces. For examples, five tetrahedra arranged symmetrically about an axis form a decahedron, and 20 tetrahedra in a three-dimensional configuration assembled about a common vertex produce an icosahedron. A strong evidence for this interpretation is the observation of the theoretically predicted notches<sup>12</sup> at the twin boundaries of a decahedron, as shown in Figure 1b. The formation mechanisms for porous nanowires and nanobrushes are still under investigation. Possible scenarios can be hydrogen evolution, the capping effect at high growth rate, or an oscillatory behavior in the nucleation kinetics that can result in branched structures.<sup>13</sup> Other electrodeposition parameters can also

affect the architecture of the mesostructures. For example, snowflake-shaped mesostructures were observed in the presence of ethanol (right panel of the graphic in Table of Contents for this Communication). Truncated mesoparticles appeared when nitric anions were partially replaced with acetic anions. As shown in the Supporting Information, high yields of these mesostructures can be produced, though more effort is needed to achieve monodisperse architectures. In summary, the abundance of controllable parameters enables electrodeposition to be a versatile and facile pathway to fabricate mesostructures with novel architectures. We also show that electrodeposition provides a convenient way to pursue the architecture-formation mechanisms of mesostructures that will enable scientists to tailor mesostructures of other emerging systems and to seek for novel fundamental phenomena and for new applications.

**Acknowledgment.** This work was supported by the U.S. Department of Energy, BES-Materials Science, Contract No. W-31-109-ENG-38. Z.L.X. also acknowledges support from the Consortium for Nanoscience Research at Argonne National Laboratory and the University of Chicago. Electron microscopy was carried out in the Electron Microscopy Center at Argonne. We are also thankful for M. P. Zach's comments.

**Supporting Information Available:** More experimental details and some SEM images at low magnifications. This materials is available free of charge via the Internet at <http://pubs.acs.org>.

## References

- (1) Mesoscopic structures are characterized by dimension scale ranging from 10 nm to micrometers. See: Penner, R. M. *J. Phys. Chem. B* **2002**, *106*, 3339–3353.
- (2) Ahmadi, T. S.; Wang, Z. L.; Green, T. C.; Henglein, A.; El-Sayed, M. A. *Science* **1996**, *272*, 1924–1926.
- (3) (a) Xu, Z.; Xiao, F. S.; Purnell, S. K.; Alexeev, O.; Kawi, S.; Deutsch, S. E.; Gates, B. C. *Nature* **1994**, *372*, 346–348. (b) Alivisatos, A. P. *Science* **1996**, *271*, 933–937. (c) Bruchez, M., Jr.; Moronne, M.; Gin, P.; Weiss, S.; Alivisatos, A. P. *Science* **1998**, *281*, 2013–2016. (d) Bezryadin, A.; Lau, C. N.; Tinkham, M. *Nature* **2000**, *404*, 971–974.
- (4) Hultheen, J. C.; Martin, C. R. *J. Mater. Chem.* **1997**, *7*, 1075–1087.
- (5) (a) Whitney, T. M.; Jiang, J. S.; Searson, P. C.; Chien, C. L. *Science* **1993**, *261*, 1316–1319. (b) Thurn-Albrecht, T.; Schotter, J.; Kastle, C. A.; Emley, N.; Shibauchi, T.; Krusin-Elbaum, L.; Guarini, K.; Black, C. T.; Tuominen, M. T.; Russell, T. P. *Science* **2000**, *290*, 2126–2129.
- (6) (a) Duan, X. F.; Huang, Y.; Cui, Y.; Wang, J. F.; Lieber, C. M. *Nature* **2001**, *409*, 66–69. (b) Gudixsen, M. S.; Lauhon, L. J.; Wang, J.; Smith, D. C.; Lieber, C. M. *Nature* **2002**, *415*, 617–620.
- (7) (a) Peng, X. G.; Manna, L.; Yang, W. D.; Wickham, J.; Scher, E.; Kadavanich, A.; Alivisatos, A. P. *Nature* **2000**, *404*, 59–61. (b) Manna, L.; Scher, E. C.; Alivisatos, A. P. *J. Am. Chem. Soc.* **2000**, *122*, 12700–12706. (c) Jun, Y. W.; Jung, Y. Y.; Cheon, J. *J. Am. Chem. Soc.* **2001**, *123*, 5150–5151. (d) Jana, N. R.; Gearheart, L.; Murphy, C. J. *J. Phys. Chem. B* **2001**, *105*, 4065–4067. (e) Puentes, V. F.; Krishnan, K. M.; Alivisatos, A. P. *Science* **2001**, *291*, 2115–2117. (f) Lee, S. M.; Jun, Y.-W.; Cho, S. N.; Cheon, J. *J. Am. Chem. Soc.* **2002**, *124*, 11244–11245. (g) Peng, X. *Adv. Mater.* **2003**, *15*, 459–463.
- (8) Sun, Y.; Xia, Y. *Science* **2002**, *298*, 2176–2179.
- (9) (a) Pan, Z. W.; Dai, Z. R.; Wang, Z. L. *Science* **2001**, *291*, 1947–1949. (b) Kong, X. Y.; Wang Z. L. *Nano Lett.* **2003**, *3*, 1625–1631.
- (10) (a) Gao, P.; Wang, Z. L. *J. Phys. Chem. B* **2002**, *106*, 12653–12658. (b) Lao, J. Y.; Wen, J. G.; Ren, Z. F. *Nano Lett.* **2002**, *2*, 1287–1292. (c) Tian, Z. R.; Voigt, J. A.; Liu, J.; Mckenzie, B.; Mcdermott, M. J.; Rodriguez, M. A.; Konishi, H.; Xu, H. *Nature Mater.* **2003**, *2*, 821–826.
- (11) Zach, M. P.; Ng, K. H.; Penner, R. M. *Science* **2000**, *290*, 2120–2123.
- (12) (a) Marks, L. D. *Philos. Mag. A* **1984**, *49*, 81–83. (b) Marks, L. D. *Rep. Prog. Phys.* **1994**, *57*, 603–649.
- (13) Fleury, V. *Nature* **1997**, *390*, 145–148.

JA0315154